RESEARCH ARTICLE

Generation of novel neuroinvasive prions following intravenous challenge

Patricia Aguilar-Calvo[1]*; Cyrus Bett[1]*; Alejandro M. Sevillano[1]; Timothy D. Kurt[1]; Jessica Lawrence[1]; Katrin Soldau[1]; Per Hammarström[2]; K. Peter R. Nilsson[2]; Christina J. Sigurdson [ID][1,3]

[1] Departments of Pathology and Medicine, UC San Diego, La Jolla, CA.
[2] Department of Physics, Chemistry, and Biology, Linköping University, Linköping, Sweden.
[3] Department of Pathology, Microbiology, and Immunology, UC Davis, Davis, CA.

Abstract

Prions typically spread into the central nervous system (CNS), likely via peripheral nerves. Yet prion conformers differ in their capacity to penetrate the CNS; certain fibrillar prions replicate persistently in lymphoid tissues with no CNS entry, leading to chronic silent carriers. Subclinical carriers of variant Creutzfeldt–Jakob (vCJD) prions in the United Kingdom have been estimated at 1:2000, and vCJD prions have been transmitted through blood transfusion, however, the circulating prion conformers that neuroinvade remain unclear. Here we investigate how prion conformation impacts brain entry of transfused prions by challenging mice intravenously to subfibrillar and fibrillar strains. We show that most strains infiltrated the brain and caused terminal disease, however, the fibrillar prions showed reduced CNS entry in a strain-dependent manner. Strikingly, the highly fibrillar mCWD prion strain replicated in the spleen and emerged in the brain as a novel strain, indicating that a new neuroinvasive prion had been generated from a previously non-neuroinvasive strain. The new strain showed altered plaque morphology, brain regions targeted and biochemical properties and these properties were maintained upon intracerebral passage. Intracerebral passage of prion-infected spleen re-created the new strain. Splenic prions resembled the new strain biochemically and intracerebral passage of prion-infected spleen re-created the new strain, collectively suggesting splenic prion replication as a potential source. Taken together, these results indicate that intravenous exposure to prion-contaminated blood or blood products may generate novel neuroinvasive prion conformers and disease phenotypes, potentially arising from prion replication in non-neural tissues or from conformer selection.

INTRODUCTION

Prion diseases are fatal neurodegenerative disorders caused by PrP^Sc, a misfolded and aggregated form of the normal cellular protein, PrP^C (1, 20, 31). During prion disease, PrP^Sc recruits and templates the misfolding of PrP^C in an autocatalytic conversion (66), an amplification process also employed by other pathogenic protein aggregates, including α-synuclein, amyloid-β and tau (19, 28, 37, 49, 52). PrP^Sc can exist in a vast array of conformers, from small subfibrillar aggregates to long fibrils visible *in situ* by electron microscopy (2, 9).

Although defined as infectious proteins, prion conformers vary profoundly in transmission between individuals and in the disease pathogenesis. While generally infectious when in direct contact with the central nervous system (CNS), for example from a prion-contaminated meningeal graft or EEG electrodes (8, 38, 39, 55),

prions differ in transmission following an extraneural exposure such as ingestion (40, 65). Certain prion conformers will replicate persistently in lymphoid tissue without accessing the CNS, resulting in lifelong subclinical carriers of infectious prions (7, 22). Understanding the conformers limited to the lymphoid tissues vs. those that will spread into the brain would provide fundamental insights into the risk of a protein aggregate breaching the CNS barrier.

How prions traffic from extraneural entry sites, such as the gastrointestinal tract, into the CNS is unresolved. Prions sequentially accumulate along neuroanatomically connected circuitry, implicating axonal transport in prion transit (3–5, 44, 46). Additionally, manipulating sympathetic nerves supplying lymphoid organs through sympathectomy or hyperinnervation reduces or accelerates prion neuroinvasion, respectively (34, 35). Recent studies have shown that prion neuroinvasion depends on the PrP^Sc conformation (10–12). "Fibrillar" prions form dense extracellular, congophilic

plaques composed of visible fibrils *in situ,* whereas "subfibrillar" prions form punctate or diffuse fine aggregates with no visible fibrils *in situ* by electron microscopy. We found a striking difference in neuroinvasion, in that the subfibrillar prions consistently neuroinvade following an intraperitoneal (IP) or intra-tongue exposure (100%), whereas the fibrillar prions rarely neuroinvade (<40%) (10, 12). Sonicating the fibrillar prions increased neuroinvasion for one strain, suggesting that prion aggregate size or particle number may limit CNS entry (12). The intravenous (IV) route has been shown to be highly efficient for prion neuroinvasion as compared with IP and subcutaneous routes (14, 43), yet the influence of prion conformation has not been previously investigated. Here we sought to understand how conformation impacts CNS entry following a hematogenous exposure.

Inadvertent prion spread by blood transfusion from prion-infected donors has been a major public health concern, particularly with the advent of lymphotrophic variant Creutzfeldt–Jakob disease (vCJD) prions resulting from bovine spongiform encephalopathy (BSE) transmission to humans (17, 25). An estimated 1:2000 individuals in the United Kingdom may harbor PrP^{Sc} in lymphoid tissues, based on the discovery of prion-positive appendices in a large-scale retrospective study (32). vCJD prions have a prominent replication phase in lymphoid tissues (61), and have been detected in the blood and urine of vCJD-infected individuals (24, 56) and form fibrillar plaques in the brain (30, 50). To date there have been four cases of human-to-human prion transmission following blood transfusion from an infected donor (51, 59, 60, 72), and an additional asymptomatic case that had received pooled plasma (59), indicating that the hematogenous route may be permissive for the neuroinvasion of these fibrillar prion conformers.

To explore the relationship between prion conformation and neuroinvasion from a blood-based exposure, we challenged mice intravenously to a conformationally diverse panel of five mouse-adapted prion strains, classified as either subfibrillar or fibrillar. We demonstrate that the subfibrillar and fibrillar prion strains penetrate the brain and replicate in the parenchyma, indicating that the hematogenous route is an efficient pathway for neuroinvasion of diverse prion strains and the only peripheral route thus far that permitted entry of the fibrillar mouse-adapted chronic wasting disease (mCWD) prion strain. Four of five prion strains appeared identically in mice exposed hematogenously or intracerebrally, indicating that the prions were capable of CNS entry. One fibrillar strain, 87V, was markedly more neuroinvasive by the IV route than the previously tested IP route. Interestingly, hematogenous exposure to the fifth prion strain, mCWD, generated a novel dominant strain that emerged in the brain after a prolonged incubation period. Lymphoid tissues can generate new strains upon cross-species prion transmission (6, 18), however new strains have not been previously generated from stable mouse-adapted strains. To test whether the source of the new strain was lymphoid tissue, we intracerebrally passaged an mCWD-infected spleen and discovered both the original strain as well as the novel strain. Together these findings indicate that (i) the hematogenous route is highly permissive to the entry of diverse prion conformers and (ii) extraneural exposure to non-neuroinvasive fibrillar prions may lead to the generation and emergence of new neuroinvasive prions, resulting in unexpected phenotypes in the brain.

MATERIALS AND METHODS

Mouse inoculations and prion strains

WT (VM/Dk) or *tg*a20 (Sv129/C57BL/6) mice (groups of n = 4–10 male and female mice, 2–3 months old) were inoculated intravenously (IV) with 50 μL or intracerebrally (IC) into the left parietal cortex with 30 μL of 1% prion-infected brain homogenate or 1% spleen homogenate from terminally ill or uninfected mice (mock). The brain homogenate was derived from IC-inoculated mice while the mCWD spleen homogenate was derived from an IP-inoculated mouse.

The ME7, 22L, 87V and RML prions are cloned strains (12, 16, 26, 27). The mCWD inoculum was the fifth passage of a single CWD-infected deer brain (12, 67).

*Tg*a20 mice express the $Prnp^a$ sequence variant and develop prion disease after a short incubation period with fibrillar mCWD (vs. >550 days in C57BL/6 mice), whereas VM/Dk mice express the $Prnp^b$ sequence variant (57) and are highly susceptible to 87V fibrillar prions (the 87V prion morphology is altered in the *tg*a20 brain). The (12, 67) subfibrillar 22L and fibrillar 87V prions were investigated in WT mice (VM/Dk), and the subfibrillar RML and 22L prions, and the fibrillar mCWD prions, were investigated in *tg*a20 mice.

Mice were maintained under specific pathogen-free conditions on a 12:12 light/dark cycle and were monitored three times weekly for the presence of terminal neurological signs of prion disease, including kyphosis, ataxia, stiff tail, hind leg clasp and hind leg paresis. Mice were euthanized at the onset of terminal disease. Spleens were removed first, with half embedded in optimal cutting temperature (OCT) and half frozen for biochemical analyses. The brain was removed and halved with a sterile blade. One hemi-brain was formalin-fixed for 2–3 days, then immersed in 96% formic acid for 1 h, washed in water, post-fixed in formalin for 2–4 days, cut into 2 mm transverse sections and paraffin-embedded for histological analysis. For the other hemi-brain, a 2–3 mm transverse section at the level of the hippocampus/thalamus was removed, embedded in OCT and immediately frozen on dry ice. The remaining brain sections were frozen for biochemical analyses.

All procedures involving animals were performed to minimize suffering and were approved by the Institutional Animal Care and Use Committee at UC San Diego. Protocols were performed in strict accordance with good animal practices, as described in the Guide for the Use and Care of Laboratory Animals published by the National Institutes of Health. Handling and import of prion infected tissue sections was performed with the approval from the Swedish Work Environment Authority and the Swedish Board of Agriculture.

Histology and immunohistochemistry

Sections of brain (4μm) were cut onto positively charged silanized glass slides and stained with hematoxylin and eosin, or immunostained using antibodies for PrP (SAF84) or for astrocytes (GFAP, glial fibrillary acidic protein). For PrP staining, sections were deparaffinized and incubated for 5 min in 96% formic acid, then washed in water for 5 min, treated with 5 μg/mL of proteinase K for 7 min and washed in water for 5 min. Sections were then placed in citrate

buffer (pH 6) and heated in a pressure cooker for 20 min, cooled for 5 min and washed in distilled water. Sections were blocked and incubated with anti-PrP SAF-84 (SPI bio; 1:400) for 45 min followed by anti-mouse biotin (Jackson Immunolabs; 1:250) for 30 min and streptavidin-horseradish peroxidase (HRP) (Jackson Immunolabs; 1:2000) for 30 min. Slides were then incubated with DAB reagent for 7 min and an enhancer for 2 min (Invitrogen). Sections were counterstained with hematoxylin. GFAP immunohistochemistry for astrocytes (1:500; DAKO) was similarly performed, however, with antigen retrieval by PK-digestion (20 μg/mL for 10 min at room temperature).

For performing the lesion profiles, eight anatomic brain regions, including dorsal medulla, cerebellum, hypothalamus, medial thalamus, hippocampus, corpus callosum, medial cerebral cortex dorsal to hippocampus and cerebral peduncle were scored for the presence of spongiosis, gliosis and PrP aggregates on a scale of 0–3 (not detectable, mild, moderate, severe). The three scores were summed and the value obtained for the lesion profile was depicted in the "radar plots" (4–10 mice per group). Two investigators blinded to animal identification performed the histological analyses.

Histoblots

Histoblots were performed as reported in Taraboulos *et al* (70), using up to 100 μg/mL of proteinase K (PK) to digest PrP^C. Histoblots were developed using the anti-PrP POM1 antibody (62).

Western blots and glycoform profiles

Brain and spleen tissue were homogenized in PBS (10% weight/volume) in new sealed tubes with new beads using a Beadbeater™ tissue homogenizer. Homogenates were digested with 50 μg/mL PK in a Tris-based lysis buffer (10 mM Tris-HCl, 150 mM NaCl, 10 mM EDTA, 0.5% NP40, 0.5% DOC; pH 7.4) at 37°C for 30 min and the reaction stopped by boiling samples for 5 min in LDS loading buffer (Invitrogen). Samples were electrophoresed through a 10% Bis-Tris gel (Invitrogen) and transferred to a nitrocellulose membrane by wet blotting. Membranes were incubated with anti-PrP monoclonal antibody POM1 [discontinuous epitope at C-terminal domain (62)] followed by incubation with an HRP-conjugated anti-mouse IgG secondary antibody. The blots were developed using a chemiluminescent substrate (ECL detection kit, ThermoScientific) and visualized on a Fuji LAS 4000 imager. Quantification of PrP^{Sc} glycoforms was performed using Multigauge V3 software (Fujifilm).

PrP^{Sc} was concentrated from the *tg*a20 mouse brain and spleen samples by performing sodium phosphotungstic acid (NaPTA) precipitation prior to western blotting (71). Briefly, aliquots of 10% brain homogenate in an equal volume of 4% sarkosyl in PBS were digested with an endonuclease [Benzonase™ (Sigma)] at 37°C for 30 min followed by treatment with 100 μg/mL PK at 37°C for 45 min. NaPTA in 170 mM MgCl$_2$ (4% NaPTA/MgCl$_2$) and protease inhibitors (Complete-TM, Roche) were added and extracts were then incubated at 37°C for 30 min and centrifuged at 18 000 × g for 30 min at 37°C. Pellets were resuspended in 0.1% sarkosyl prior to electrophoresis and blotting.

Thermal denaturation assay

Brain homogenate in a Tris lysis buffer (10 mM Tris-HCl pH 7.4, 150 mM NaCl, 2% sarcosyl) was digested with 100 μg/mL PK for 40 min at 37°C. PK was inactivated with phenylmethylsulfonyl fluoride (PMSF) (2 mM final concentration). Sodium dodecyl sulfate (SDS) (2.1% final) was added to the samples and samples were heated to temperatures ranging from 25°C to 99°C (10° intervals) for 6 min with shaking in a thermomixer set at 1000 rpm. Western blotting was performed and PrP signals from monomers were captured and quantified using a Fujifilm LAS-4000 imager and Multigage software. Strains were analyzed in 3 independent experiments using 4 mice per strain.

h-FTAA staining and fluorescence life time imaging

Sections of OCT-embedded brain samples (10μm) were cut onto positively charged silanized glass slides, dried for 1 h and fixed in 100% then 70% ethanol for 10 min each. After washing with deionized water, sections were equilibrated in phosphate buffer saline (PBS), pH 7.4, for 10 min. h-FTAA was diluted in PBS to a final concentration of 1.5 μM and added to the sections. The sections were incubated with h-FTAA for 30 min at room temperature, washed with PBS and mounted using DAKO fluorescence mounting medium. The fluorescence decay of h-FTAA bound to PrP aggregates was collected using an inverted Zeiss (Axio Observer.Z1) LSM 780 microscope (Carl Zeiss MicroImaging GmbH) equipped with a modular fluorescence lifetime imaging (FLIM) system from Becker and Hickl. In this setup, the emitted photons were routed through the direct coupling (DC) confocal port of the Zeiss LSM 780 scanning unit and detected by a Becker and Hickl HPM-100-40 hybrid detector. Data were recorded by a Becker and Hickl Simple-Tau 152 system (SPC-150 TCSPC FLIM module) with the instrument recording software SPCM version 9.42 in the FIFO image mode, 256 × 256 pixels, using 256 time channels (Becker and Hickl GmbH). For all acquisitions, a T80R20 main beam splitter was used and the pinhole was set to 20.2 μm. Scanning area was set to 235.7 μm × 235.7 μm, with a scanning resolution of 512 × 512 pixels. A Plan-Apochromat 40 ×/1.3 Oil DIC objective lens was used and a 510 nm longpass filter was positioned in front of the hybrid PMT. Excitation utilized the 490 nm laser line from the pulsed tunable In *Tune* laser (Carl Zeiss MicroImaging GmbH) with a repetition rate of 40 MHz. Data was subsequently analyzed in SPCImage version 3.9.4 (Becker and Hickl GmbH), fitting each of the acquired decay curves to a tri-exponential function and color coded images, as well as distribution histograms, showing the intensity-weighted mean lifetimes generated with the same software. The procedure of staining and FLIM imaging protein aggregates with h-FTAA is described in detail in Reference (58).

RESULTS

Fibrillar prions invade the CNS following an IV exposure, but with a low attack rate

Certain fibrillar prions (87V, mCWD) rarely neuroinvade from the peritoneal cavity or from the tongue (12). To test the efficiency of fibrillar prion entry into the CNS from the hematogenous route, we
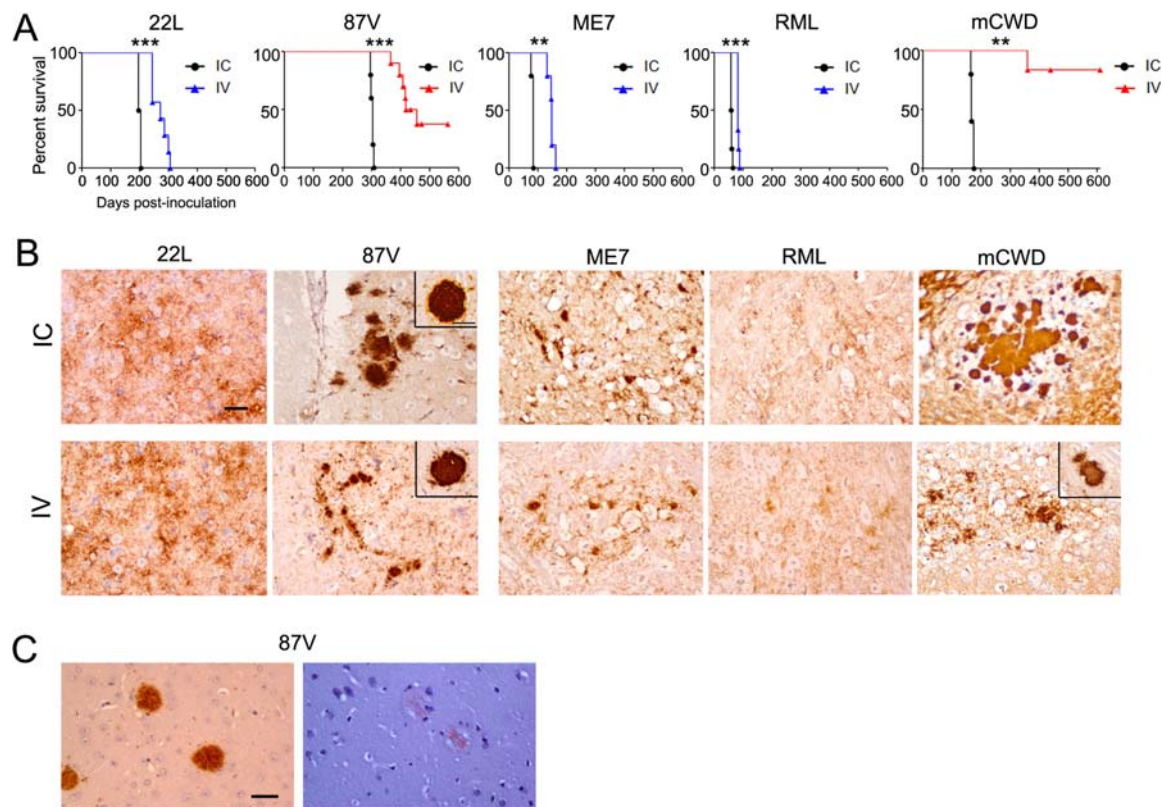
Figure 1. *Neuroinvasion of subfibrillar and fibrillar prions following an intravenous exposure.* **A.** Survival curves of VM/Dk mice inoculated with subfibrillar 22L or fibrillar 87V prions, and *tga*20 mice inoculated with subfibrillar ME7, RML or fibrillar mCWD prion strains by the IC or IV route. Shown are the times to terminal prion disease. **B.** Brain immunolabeled for PrP shows a similar prion aggregate morphology in mice inoculated by the IC or IV route for 22L, 87V, ME7 and RML prions, but not for mCWD prions. Insets show examples of the dense plaques seen in the 87V-inoculated VM/Dk mice, and a rare dense plaque in an mCWD IV-exposed *tga*20 mouse. **C.** PrP immunolabeling (left panel) and Congo red stain (right panel) of dense 87V plaques in an IV-inoculated mouse. Group numbers were as follows: 22L: n = 4 IC, n = 7 IV; 87V: n = 5 IC, n = 10 IV; ME7: n = 5 IC and IV; RML: n = 6 IC and IV; mCWD: n = 5 IC, n = 6 IV. Log-rank (Mantel–Cox) test for survival in panel A, **$P < 0.01$, ***$P < 0.001$. Scale bar = 50 μm.

inoculated subfibrillar or fibrillar prions, or uninfected brain (mock), intravenously and assessed mice for prion aggregates in the spleen and brain. *Tga*20 mice overexpress mouse PrP and were used to compare subfibrillar RML and ME7 to the fibrillar mCWD prions as the incubation period for mCWD in wild type mice is prohibitively long for studies of prion spread from peripheral inoculation routes. Wild type mice (VM/Dk background) were used to compare the subfibrillar 22L and the fibrillar 87V prion strains, as the 87V forms fibrils in the VM/Dk mice, but not in *tga*20 mice (detailed in Methods).

All five prions were detected in the spleen by early timepoints post-inoculation. Typically only a few follicles showed PrP^{Sc} deposition (Supporting Information Figure S1), consistent with reports of early prion replication in lymphoid tissues in prion-infected mice, sheep and deer (41, 47, 68).

All subfibrillar prions, 22L, ME7 and RML, readily spread to the CNS, inducing clinical prion disease with a 100% attack rate. The incubation period to terminal disease was delayed by 40%–80% as compared with the IC route (Figure 1A). In contrast, the fibrillar prions induced terminal prion disease with only a 17% or 60% attack rate for mCWD or 87V prions, respectively. Terminal disease was delayed by a longer period for mCWD (110%) than for

87V (35%) as compared with the IC route (Figure 1A) (Table 1). For mCWD, an IV exposure led to a similar low attack rate as compared with the previously tested IP route, whereas 87V was markedly more neuroinvasive by the IV route than by the IP route (previously 0% attack rate) (10). Neither mCWD nor 87V prions previously induced fibrillar plaques in the brain when inoculated IP, yet both strains transited into the CNS, when inoculated IV.

Subfibrillar and 87V fibrillar prions neuroinvade and maintain their original biological properties, while mCWD fibrillar prions diverge from the original strain

Prion aggregates associated with a strain may consist of more than one conformer. To determine whether the conformers introduced hematogenously varied from those introduced intracerebrally, we compared prion deposits in the brain after an IC or IV exposure by immunohistochemistry and western blot. For the subfibrillar strains, 22L, ME7 and RML, the aggregates ranged from a diffuse distribution of fine PrP^{Sc} deposits of less than 1 μm to small 5–10 μm plaques, whereas for the fibrillar 87V strain, aggregates ranged from diffuse deposits in the thalamus to large plaques (20–60 μm) in the

Table 1. Disease phenotype in *tga*20 mice inoculated with mCWD.

Inoculum	Inoculation route	Animal no.	Incubation period (dpi)	PrP^{Sc} dominant glycoform*	Plaque morphology
Brain	IC	1	165	Mono	Large,[†] dense plaques in corpus callosum
		2	167	Mono	Large, dense plaques in corpus callosum
		3	167	Mono	Large, dense plaques in corpus callosum
		4	174	Mono	Large, dense plaques in corpus callosum
		5	174	Mono	Large, dense plaques in corpus callosum
Brain	IV	1	440	Neg[¶]	Negative
		2	360§	Di	Diffuse punctate aggregates;** 2 plaques
		3	609	Neg	Negative
		4[‡]	609	Neg	Diffuse punctate aggregates[††]
		5	609	Di	Diffuse punctate aggregates; 1 plaque
		6	609	Neg	Diffuse punctate aggregates
Brain	IV-to-IC	1	342	Di	Diffuse punctate aggregates; 3 small plaques
		2[‡‡]	373	Di	Diffuse punctate aggregates; 1 plaque
		3[¶¶]	376	Di	Diffuse punctate aggregates
		4	419	Di	Negative
		5	452	Neg	Diffuse punctate aggregates
Spleen	IC	1	242	Di	Diffuse punctate aggregates; 1 plaque
		2	254	Di	Diffuse punctate aggregates; 1 plaque
		3	256	Di	Large, dense plaques in corpus callosum
		4	256	Mono	Diffuse punctate aggregates; multiple plaques
		5	280	Di	Large and small dense plaques

*PrP^{Sc} glycoform were assessed from immunoblotting of PK-digested brain and spleen homogenates.

†Plaques were >20 μm.

‡Brain used for subpassage (IV-to-IC).

§Mouse showed clinical signs of prion disease.

¶Negative for PrP^{Sc} by Western blot.

**Punctate aggregates were 2–4 μm.

††Brain PrP^{Sc} shown in Figure 1B.

‡‡Brain shown in Online Resource 2b (thermostability).

¶¶Brain shown in Figure 5B (h-FTAA image).

cortex (Figure 1B). For these four prions (22L, ME7, RML and 87V), mice exposed by the IC or IV route showed an indistinguishable prion aggregate morphology in the brain (Figure 1B), including the congophilic plaques of 87V prions (Figure 1C). In contrast, mice exposed IC or IV to mCWD prions developed aggregates that differed markedly in brain; after IV exposure, there were primarily clusters of 2–3 μm punctate aggregates and two 15 μm dense plaques, whereas after IC exposure, there were only large, dense 20–100 μm plaques (Figure 1B). PrP^{Sc} deposits were present in 4 of 6 mCWD IV-exposed mice, 3 of which did not develop terminal signs of prion disease. Interestingly, the mCWD aggregates deposited in the corpus callosum following either an IV or IC exposure.

Within a strain, PrP^{Sc} typically maintains a consistent biochemical signature, including electrophoretic mobility and glycoform profile (distribution of di-, mono- and unglycosylated isoforms). In addition to inducing similar histological properties in the brain, four of five prions (22L, ME7, RML and 87V) showed an indistinguishable PrP^{Sc} electrophoretic mobility and glycoform profile in mice inoculated by either the IC or IV route (Figure 2A). Remarkably, for mCWD, the PrP^{Sc} glycoprofile differed between the IC- and IV-inoculated mice, as the latter showed a relative increase in diglycosylated PrP^{Sc} and a decrease in unglycosylated PrP^{Sc} (Figure 2B).

IV exposure to mCWD fibrillar prions leads to a new dominant prion strain

To further determine whether a new dominant mCWD prion strain had been generated following an IV prion exposure, we subpassaged the brain from the mCWD- and 87V-IV-infected mice by IC inoculation of naïve mice (IV-to-IC). For the 87V strain, mice developed prion disease with a modest but significant decrease in the incubation period compared with the original strain (17% reduction), whereas for the mCWD strain, the incubation period markedly increased by 104% (Figure 3A,B). For 87V, the plaque morphology appeared identical to the original strain, including dense congophilic plaques (Figure 3C). For mCWD, however, two types of prion deposits were detected, large, dense plaques typical of IC-inoculated mice and small 2–6 μm aggregates, similar to those seen in the IV-inoculated mice. The small plaques localized in part in the corpus callosum, suggesting some fundamentally similar properties to the original strain (Figure 3D).

We next compared the lesion distribution in mice that were IC-inoculated with the original strain vs. the IV-to-IC subpassaged strain by scoring spongiform change, gliosis and PrP^{Sc} deposition levels in 8 brain regions. For 87V, the distribution and severity of the lesions following IV-to-IC subpassage were similar to the lesions
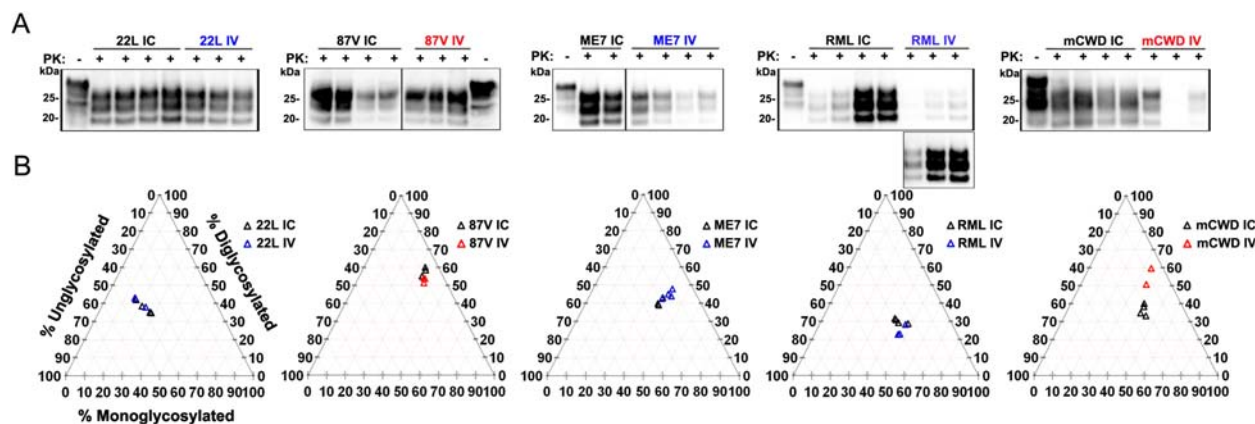
Figure 2. *Biochemical properties of subfibrillar and fibrillar prions in the brain following IC or IV inoculation.* **A.** Western blots of brain revealed no differences in the PrP^{Sc} electrophoretic mobility in the VM/Dk mice exposed to 22L or 87V prions, or in *tga*20 mice exposed to ME7, RML or mCWD prions by the IC or IV route. A higher exposure of the same membrane is shown for RML. For the 87V and ME7 blots, a lane was removed from the membrane. **B.** Triplots of the relative di-, mono- and unglycosylated PrP^{Sc} levels revealed similar glycoform patterns for 22L, 87V, ME7 and RML prions for the IC or IV routes. IV-inoculated mCWD showed a relative increase in diglycosylated PrP^{Sc} and a decrease in unglycosylated PrP^{Sc} as compared with the IC-inoculated mCWD. N= 3–5 mice per strain and inoculation route. For IV-inoculated mCWD, only 2 of 5 animals were positive for PrP^{Sc} by western blot (numbers 2 and 5 in Table 1).

induced by the original 87V prions IC (Figure 3E). Yet for mCWD, a marked decrease in the PrP^{Sc} deposition, as well as an overall decrease in the gliosis led to a decrease in the lesion severity observed in the IV-to-IC subpassage mice as compared with the original mCWD prions (Figure 3F).

To investigate the biochemical properties of the subpassaged 87V and mCWD prions, the electrophoretic mobility and glycoform profile of PK-digested PrP^{Sc} were assessed. For 87V, there was no change in the PrP^{Sc} mobility or glycoform profile in the IV-to-IC subpassaged vs. original 87V strain (Figure 4A). For mCWD, the electrophoretic mobility was unchanged, but the glycoprofile of the IV-to-IC subpassaged prions again differed, with a significant increase in diglycosylated PrP^{Sc} and a decrease in the unglycosylated PrP^{Sc} (Figure 4B), suggesting that a new strain emerged from the IV inoculation.

The thermostability of 87V and mCWD IC and IV-to-IC subpassaged brains was also assessed by quantifying levels of PrP disassembly into monomers at temperatures from 25°C to 99°C. The 87V and mCWD IC prions in brain were highly thermostable as previously reported ($T_{1/2} = 85$°C) (10). Additionally, the thermostability of 87V IC and IV-to-IC prions revealed no differences in the temperature in which half of the total PrP^{Sc} aggregates disassembled into monomers ($T_{1/2} = 85$°C), again suggesting that the dominant conformers had not changed (Supporting Information Figure S2). One of five mCWD IV-to-IC brains harbored enough PrP^{Sc} to assess the thermostability, and revealed a similarly high thermostability ($T_{1/2} = 85$°C) as the mCWD from the IC inoculated mice (Supporting Information Figure S2).

Fluorescence lifetime imaging of h-FTAA bound to prion plaques

As an independent measure of prion conformation, we tested the binding properties of a conformationally sensitive luminescent probe, heptameric formic thiophene acetic acid (h-FTAA), to 87V and mCWD plaques. FLIM of h-FTAA has been previously assessed for optical distinction of PrP deposits associated with specific prion strains (53). Using FLIM, the decay of emitted light from plaque-bound h-FTAA is measured as an indicator of how h-FTAA binds to the aggregate, since the fluorescence decay of the dye is sensitive to the surrounding chemical environment. For the 87V strain, the h-FTAA fluorescence decay revealed three distinct time decay curves, corresponding to different plaque morphologies. The compact core and fibrillar plaques showed similar signatures in the 87V original strain IC and the IV-to-IC subpassage (Figure 5A). Similarly, the diffuse plaques in the thalamus showed a comparable signature of h-FTAA fluorescence decay (Figure 5A). Interestingly, the decay curves varied significantly for the three aggregate morphologies, the compact core, fibrillar and diffuse deposits, suggesting that h-FTAA binds in a different fashion to each of these aggregates. Although these distinct morphologies have been recognized for the 87V strain for decades, these data are the first indication that the aggregates may vary at the structural level.

In contrast to the 87V prions, we found clear differences between the original mCWD strain and the new neuroinvasive mCWD strain, in that the fluorescence decay was significantly faster for the new strain (Figure 5B). Curiously, both the large and small mCWD aggregates from the new neuroinvasive mCWD strain exhibited the same FLIM profile. Thus, h-FTAA binds in different fashion to the new neuroinvasive mCWD strain, suggesting that the new aggregates have an alternate structure compared with the original mCWD plaques.

mCWD prion replication in the spleen maintains the fidelity of the original strain and also generates a novel strain

The origin of the new mCWD strain was unclear, as the aggregates have not been previously observed in mice inoculated with mCWD
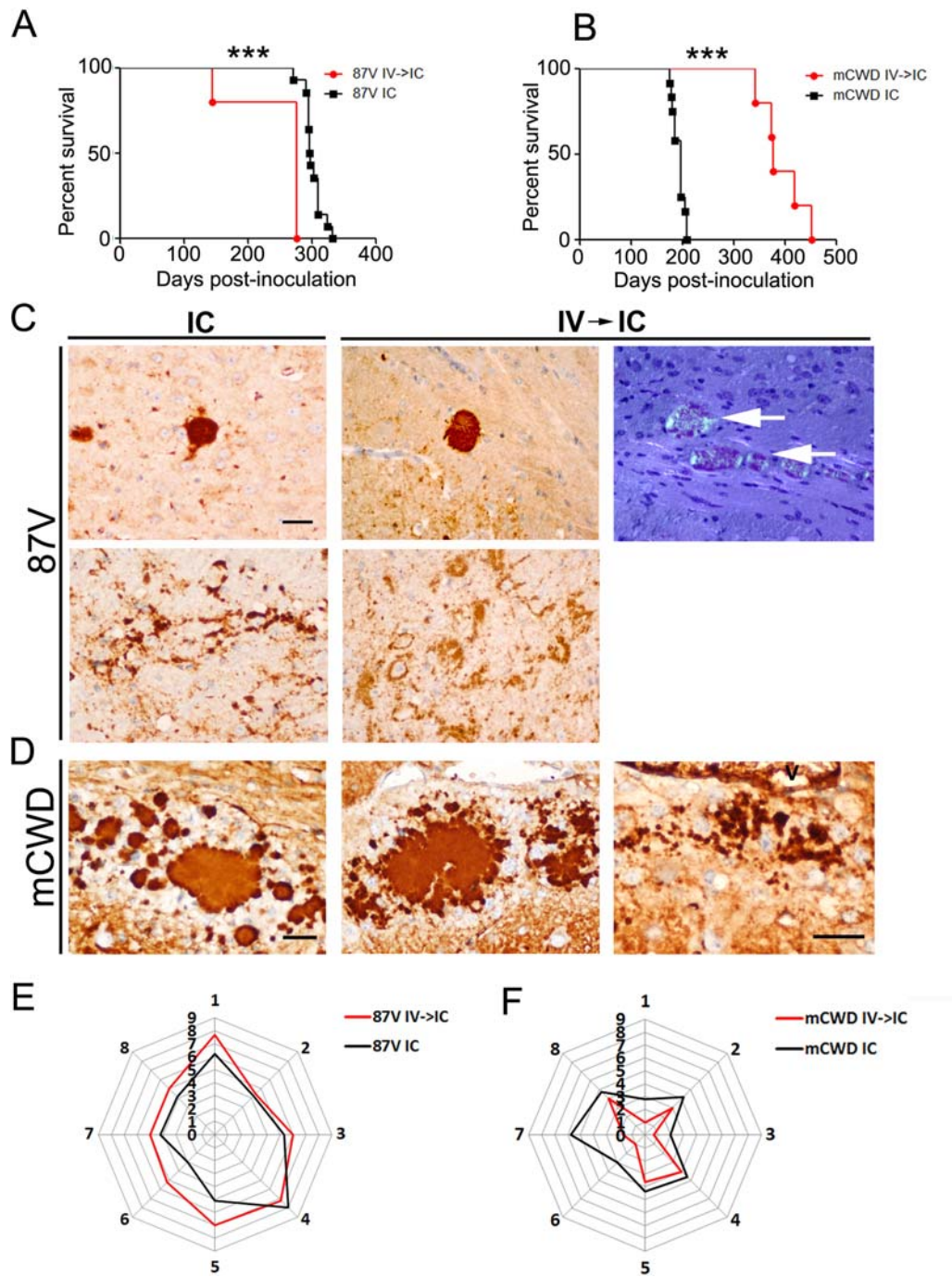
Figure 3. *Intracerebral sub-passage of 87V and mCWD IV-infected brain (IV-to-IC).* **A,B.** Survival curves of VM/Dk and *tga*20 mice inoculated IC with the brains from 87V or mCWD IV-inoculated mice, respectively. The IC route is shown for comparison. **C.** Similar dense, congophilic prion plaques and smaller deposits were detected in the 87V IC-inoculated inoculated and 87V IV-to-IC inoculated brains. **D.** Prion immunolabeling of the IV-to-IC inoculated mice showed both small punctate aggregates and large plaques, as compared with only the large plaques in the brains inoculated with original mCWD strain IC. Shown is brain from mouse 2 (PrP^{Sc} glycoform pattern shown in Figure 4B). **E.** Lesion profile of mice inoculated with 87V and **(F)** mCWD by the IC (black) or the IV-to-IC subpassage (red). The severity of spongiosis, astrogliosis and PrP^{Sc} deposition were scored for eight brain regions (1: dorsal medulla, 2: cerebellum, 3: hypothalamus, 4: medial thalamus, 5: hippocampus, 6: medial cerebral cortex dorsal to hippocampus, 7: corpus callosum and 8: cerebral peduncle) and were nearly superimposable for 87V, whereas for mCWD the severity was reduced in the IV-to-IC subpassage brain. Group numbers were as follows: 87V: n = 14 IC, n = 5 IV-to-IC; mCWD: n = 12 IC, n = 5 IV-to-IC. Log-rank (Mantel–Cox) test for survival in panel A, ***$P < 0.001$. Scale bar = 50 μm.
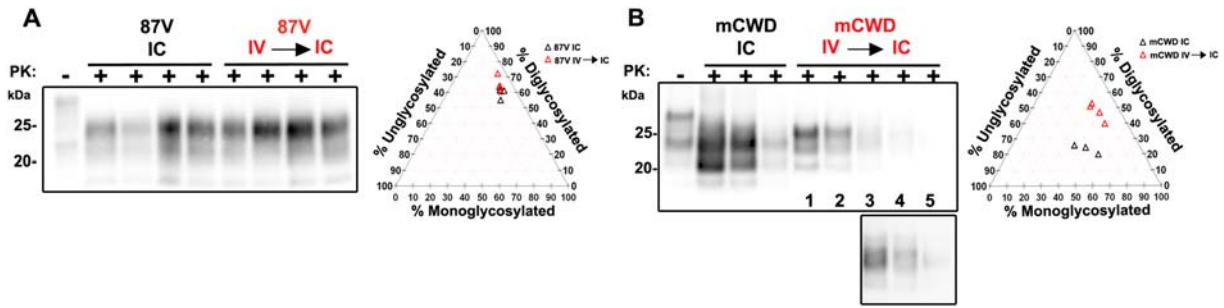
Figure 4. *Glycoprofile of 87V and mCWD IV-to-IC subpassaged prions.* **A.** Electrophoretic mobility and glycoprofile of 87V or **(B)** mCWD PrP^Sc in brains of VM/Dk or *tga*20 mice, respectively. Triplots show the relative levels of each PrP^Sc glycoform. The IV-to-IC mCWD PrP^Sc shows an increase in diglycosylated PrP^Sc and a decrease in the unglycosylated PrP^Sc compared with the original IC-inoculated mCWD. Two-way ANOVA with Bonferroni post-test for glycoforms comparison in panel B: mCWD brain IC vs. IV-to-IC: diglycosylated PrP^Sc, $P < 0.05$. Quantified data in triplots are from 3 to 4 mice per strain and inoculation route.

by the IC route. We reasoned that the new dominant mCWD strain may have been a neuroinvasive substrain present in low abundance within the original inoculum and was selected following prion exposure by the IV route. However, this neuroinvasive substrain was not observed following an intra-tongue exposure to mCWD prions (12), which would have been expected if a neuroinvasive

strain selection occurred. Alternatively, hematogenously introduced prions would have massively exposed the spleen, potentially generating a lymphoid-derived prion strain within the new replication environment. Prion strains in the spleen appear similar histologically, accumulating as diffuse aggregates in the germinal centers (Supporting Information Figure S1). To determine the nature of the
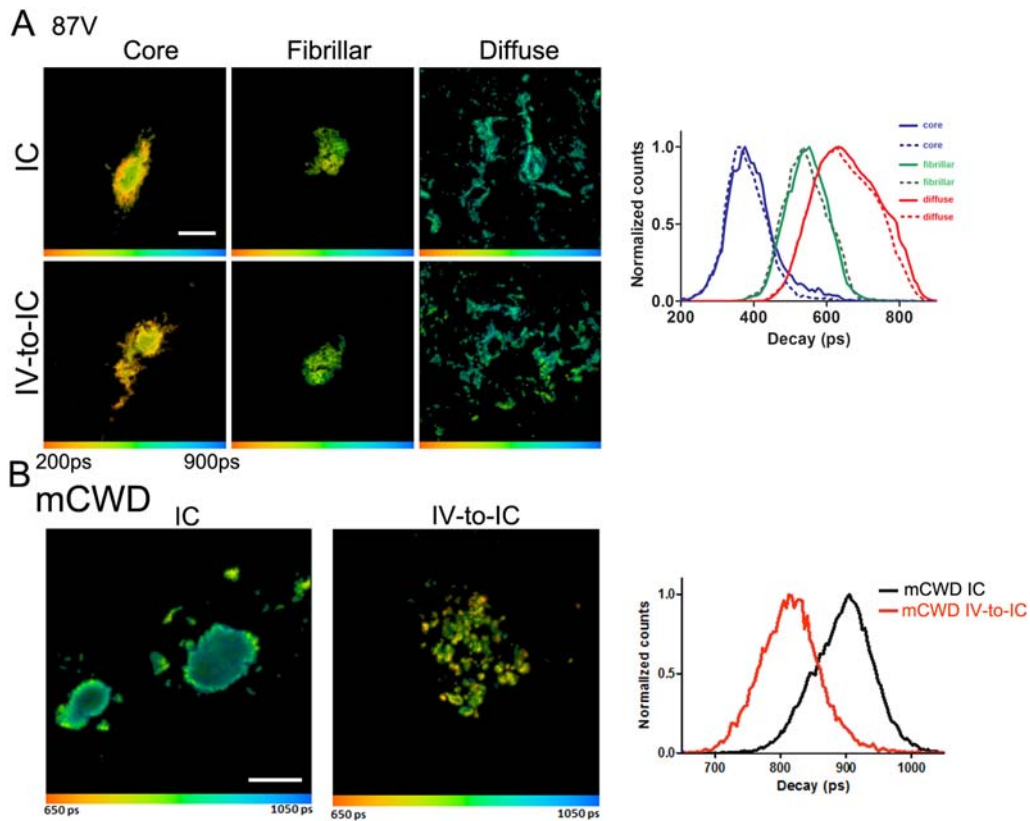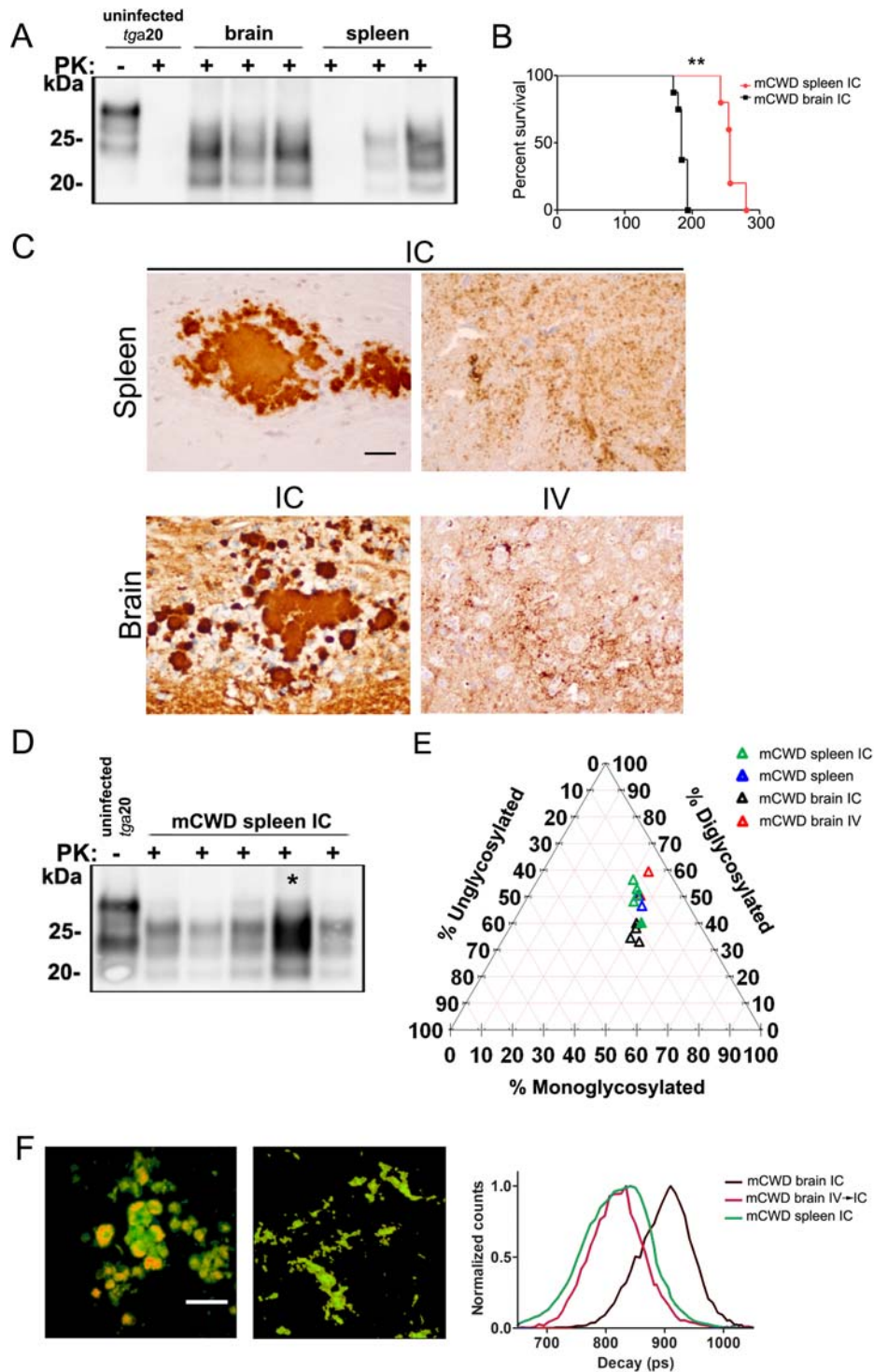

Figure 5. *Fluorescence life-time decay of h-FTAA-labeled 87V and mCWD prion plaques.* **A.** h-FTAA labeled brain cryosections from mice inoculated with the original 87V IC or 87V IV-to-IC both show three distinct aggregate morphologies with three different decay times. The three aggregate types showed nearly identical fluorescence life-time decay curves in VM/Dk mice inoculated with 87V IC (solid line) or 87V IV-to-IC (dashed line) brain homogenate. **B.** h-FTAA labeled brain cryosections show different colors and decay times for the large original mCWD IC plaques and the small punctate mCWD IV-to-IC aggregates (right; mouse number 3 in Figure 4B and in Table 1). Scale bar = 20 μm.

mCWD prions replicating within the spleen, we compared the PrP^Sc glycoform pattern in spleens and brains from mice inoculated IV or IC, respectively. Surprisingly, the dominant glycoform differed dramatically, in that the spleen showed predominantly diglycosylated PrP^Sc, whereas the brain showed predominantly monoglycosylated PrP^Sc (Figure 6A,E). Additionally, the three

PK-resistant PrP glycoforms in the spleen appear to be smaller than those in the brain (Figure 6A), also suggesting a conformational difference.

To assess the nature of splenic PrP^Sc after an extraneural exposure to mCWD, we intracerebrally inoculated a mCWD-infected spleen (from a mouse previously exposed intraperitoneally to

Figure 6. *mCWD-infected spleen harbors original and novel prion conformers.* **A.** PrP^{Sc} glycoform pattern of mCWD-infected brain and spleen shows a dominant monoglycosylated PrP^{Sc} in the brain (IC exposed) vs. diglycosylated PrP^{Sc} in the spleen (IV exposed), respectively (plotted in panel E). **B.** Survival curves of *tga*20 mice inoculated IC with mCWD-infected brain (n = 8) or spleen (n= 5). **C.** PrP labeled aggregates in brain from a spleen-inoculated *tga*20 mouse shows large dense prion plaques typical of the original mCWD IC (left upper panel, mouse 4 in panel D) and 2–3 μm punctate deposits similar to those in the IV-infected mice (right upper panel, mouse 2 in panel D). **D.** PrP^{Sc} glycoform pattern of brain from the spleen inoculated mice shows a similar banding pattern among the mice, except animal 4, which shows more equal levels of di- and mono-glycosylated PrP^{Sc} (asterisk). **E.** Triplots reveal a similar brain PrP^{Sc} glycoform profile in *tga*20 mice inoculated IC with mCWD-infected spleen (green) and IV with mCWD brain (red), which is almost identical to that of spleen

mCWD) (Figure 6B). Interestingly, the brain showed a co-occurrence of large dense prion plaques identical to the original mCWD strain IC, as well as 2–3 μm punctate PrP^{Sc} deposits similar to the mCWD prions observed in the brain after an IV exposure (Figure 6C). These data indicate that mCWD prion replication in the spleen could maintain the fidelity of the original fibrillar mCWD strain as well as generate a new prion strain. Biochemically, the spleen-derived prions in the brain showed a predominant diglycosylated PrP^{Sc} glycoform (Figure 6D,E, green triangles) that was similar in 4 of 5 mice to (i) the new mCWD prion strain that had developed after IV-inoculation of mCWD (Figure 6E, red triangles) and (ii) the mCWD prions in the spleen after IV-inoculation (Figure 6E, blue triangles).

To further assess whether the small aggregates and the larger plaques resembled the prions that developed after IV exposure to mCWD, we investigated the spleen-derived prions in brain by h-FTAA fluorescence life-time decay using FLIM. Here we found that the distribution of fluorescence life-times for h-FTAA bound to the spleen-derived prions was remarkably similar to the life-times obtained for the novel mCWD strain (Figure 6F) and there was no difference in the decay between the smaller and larger aggregates, suggesting that the novel strain may have arisen during replication in the spleen or other lymphoid tissue.

DISCUSSION

Prion conformers markedly differ in neuroinvasion efficiency from all routes tested to date, IP (10, 15), IT (12) and IV; subfibrillar prions are highly neuroinvasive, whereas fibrillar prions are poorly neuroinvasive. Among the fibrillar prions (87V and mCWD), we found striking differences in neuroinvasion when comparing the exposure routes, with the most efficient brain entry occurring from the hematogenous route. For 87V prions, the attack rate after an IV exposure far exceeded the rate that we previously reported after an IP exposure (60% vs. 0%), a marked difference considering the two-fold higher dose for the IP route (10). For mCWD prions, fibrillar plaques had not previously developed in the brain of any mouse exposed by the intra-tongue (IT) or IP route, even after fibril sonication (12). However, here mCWD prions were neuroinvasive following an IV exposure, and revealed mostly focal clusters of granular aggregates and only two small dense plaques. In humans,

PrP^{Sc} (blue). Mouse 4 (spleen IC, solid green triangle) shows a similar glycoform profile as the mice inoculated IC with original mCWD (brain IC, black). Quantified data in triplots are from 3 to 4 mice per strain and inoculation route. The mCWD IC and IV are also shown in Figure 2 and are included here for comparison. **F.** Brain cryosections stained with h-FTAA and imaged using FLIM show the dense aggregates and diffuse plaques of spleen-derived mCWD prions. The fluorescence life-time decay (right panel) shows that the curves from spleen-derived prion aggregates are similar to the subpassaged mCWD IV-to-IC prion aggregates. The mCWD brain IC and IV-to-IC are also shown in panel E and are included here for comparison. Scale bar = 50 μm (panel C) or 20 μm (panel F). Log-rank (Mantel-Cox) test for survival in panel B, $**P < 0.001$. Two-way ANOVA with Bonferroni post-test for glycoform comparison (panel E): mCWD brain IC vs. spleen IC: diglycosylated $***P < 0.001$; unglycosylated $*P < 0.05$.

prions also neuroinvade following an IV exposure and form fibrils in the brain, as four cases of transfusion-derived vCJD transmissions have occurred (51, 59, 60, 72), and brain lesions in the single patient examined histologically appeared similar to other vCJD cases with florid prion plaques (72). Thus in both experimental models and in humans, certain fibrillar prion subtypes are brain penetrant following a hematogenous exposure, and as reported here, the aggregate morphology may vary from that observed following other entry routes.

How do prions neuroinvade following an IV exposure? Prions may enter through nerve endings, for example through the sympathetic nerves innervating blood vessels or splanchnic nerves innervating the spleen, as proposed for IP introduced prions (13, 43, 64). An extensive pathogenesis study using RML prions compared the IV, IP and subcutaneous (SC) exposure routes and showed that all routes led to an early prion replication phase in the spleen, followed by replication in the spinal cord by approximately 40% of the incubation period, and lastly replication in brain (43). The incubation period was largely determined by the PNS and CNS phase, as prions replicated in the lymphoid tissue only briefly (days to a few weeks) prior to nervous system entry (45). Other studies of subfibrillar strains also support prion transit via nerves (33–35, 64). The fibrillar mCWD strain does not spread to brain following an IT or IP inoculation, suggesting that mCWD prions cannot readily transit in nerves (10, 12).

A second possibility is that prions entered the CNS directly from the blood. Direct prion passage across the blood–brain barrier (BBB) or blood–CSF barrier (BCB) following a hematogenous exposure would be expected to result in a short incubation period, comparable to the IC route. However, the long delay observed for all strains for the IV as compared with the IC route suggests that prions do not directly cross the BBB or BCB; instead, prions may replicate initially in cells such as follicular dendritic cells in lymphoid tissues or even brain endothelial or ependymal cells. Fibrillar GPI-anchorless prions were shown to be poorly CNS penetrant unless the BBB was compromised, enabling prion entry (48). An IV prion exposure of mice expressing GPI-anchorless PrP^{C} led to fibrillar GPI-anchorless prions accumulating adjacent to the meninges, and rarely within the choroid plexus, which may suggest entry across the BCB (48). However, a meningeal distribution of prions was not observed in mice in the present study.

Finally, prion penetration of the CNS for certain fibrillar conformers may require strain mutation, which is a stable switch in prion conformation from replication in a new environment (36). Strain mutation may occur either from selection of a sub-strain from a "cloud" of pre-existing conformers or from deformed templating in the presence of new co-factors (21, 29, 36, 54). We found that a new strain emerged in the brain following IV exposure to mCWD prions, potentially from strain mutation from either mechanism. The new strain was maintained on passage in mice and showed a marked alteration in the disease phenotype compared with the original strain, including a prolonged survival period and a switch in the prion aggregate morphology, lesion profile, h-FTAA-plaque bound fluorescence decay, as well as an altered PrP^{Sc} glycoform profile in the brain, which was similar to that of mCWD in the spleen. Moreover, the new phenotype could be re-created by inoculating an mCWD-infected spleen IC, revealing the spleen or other lymphoid tissue as a potential source of the new strain, and indicating that potentially any route leading to mCWD replication in the spleen may generate a new neuroinvasive strain.

Collectively, these findings indicate that the IV exposure route is a more efficient mechanism of neuroinvasion for only a subset of fibrillar prions. Additionally, prions transmitted in the blood may generate new neuroinvasive prions through strain mutation in lymphoid tissues. These new prion conformers may induce a completely new phenotype, clinically, histologically and biochemically, even though the strain originates from a previously adapted strain. Consistent with our findings, mice and non-human primates (macaques) transfused with blood products and soluble brain from vCJD-infected donors developed a prion disease, although with brain and spinal cord lesions that were distinct from those observed in animals challenged with vCJD brain inocula (23). The macaques developed an unusual clinical disease characterized by progressive proximal paresis of the forelimbs and hind limb ataxia and showed histologic features of a myelopathy. Although PrP aggregates were not detectable in the affected macaques, the disease was transmissible to mice and the mice developed prion deposits in the CNS, suggesting the presence of an atypical prion (23).

sCJD prion subtypes co-occur in the brain (63), yet the origin of the subtypes is unknown. The replication of prions by different cell types within the brain or by non-neural cells, in which the replication environment and PrP^{C} glycan sialylation patterns differ, may induce strain mutation events and help explain the origin of multiple co-existing subtypes (42, 69). Studies to identify the cellular co-factors that underlie the generation of new prion strains are ongoing.

ACKNOWLEDGMENTS

REFERENCES

1. Aguzzi A, Lakkaraju AK (2016) Cell biology of prions and prionoids: a status report. *Trends Cell Biol* **26**:40–51.
2. Bartz JC (2016) Prion strain diversity. *Cold Spring Harb Perspect Med* **6**:a024349.
3. Beekes M, Baldauf E, Diringer H (1996) Sequential appearance and accumulation of pathognomonic markers in the central nervous system of hamsters orally infected with scrapie. *J Gen Virol* **77**:1925–1934.
4. Beekes M, McBride PA (2000) Early accumulation of pathological PrP in the enteric nervous system and gut-associated lymphoid tissue of hamsters orally infected with scrapie. *Neurosci Lett* **278**:181–184.
5. Beekes M, McBride PA (2007) The spread of prions through the body in naturally acquired transmissible spongiform encephalopathies. *febs J* **274**:588–605.
6. Beringue V, Herzog L, Jaumain E, Reine F, Sibille P, Le Dur A *et al* (2012) Facilitated cross-species transmission of prions in extraneural tissue. *Science* **335**:472–475.
7. Beringue V, Le Dur A, Tixador P, Reine F, Lepourry L, Perret-Liaudet A *et al* (2008) Prominent and persistent extraneural infection in human PrP transgenic mice infected with variant CJD. *PLoS One* **3**:e1419.
8. Bernoulli C, Siegfried J, Baumgartner G, Regli F, Rabinowicz T, Gajdusek DC, Gibbs CJ Jr. (1977) Danger of accidental person-to-person transmission of Creutzfeldt-Jakob disease by surgery. *Lancet* **309**:478–479.
9. Bessen RA, Kocisko DA, Raymond GJ, Nandan S, Lansbury PT, Caughey B (1995) Non-genetic propagation of strain-specific properties of scrapie prion protein. *Nature* **375**:698–700.
10. Bett C, Joshi-Barr S, Lucero M, Trejo M, Liberski P, Kelly JW *et al* (2012) Biochemical properties of highly neuroinvasive prion strains. *PLoS Pathog* **8**:e1002522.
11. Bett C, Kurt TD, Lucero M, Trejo M, Rozemuller AJ, Kong Q *et al* (2013) Defining the conformational features of anchorless, poorly neuroinvasive prions. *PLoS Pathog* **9**:e1003280.
12. Bett C, Lawrence J, Kurt TD, Orru C, Aguilar-Calvo P, Kincaid AE *et al* (2017) Enhanced neuroinvasion by smaller, soluble prions. *Acta Neuropathol Commun* **5**:32.
13. Bondiolotti G, Rossoni G, Puricelli M, Formentin E, Lucchini B, Poli G *et al* (2010) Changes in sympathetic activity in prion neuroinvasion. *Neurobiol Dis* **37**:114–117.
14. Brown KL, Gossner A, Mok S, Mabbott NA (2012) The effects of host age on the transport of complement-bound complexes to the spleen and the pathogenesis of intravenous scrapie infection. *J Virol* **86**:25–35.
15. Bruce ME (1985) Agent replication dynamics in a long incubation period model of mouse scrapie. *J Gen Virol* **66**:2517–2522.
16. Bruce ME, Dickinson AG (1979) Biological stability of different classes of scrapie agent. In: *Slow Virus Infections of the Central Nervous System*. SB Prusiner, WH Hadlow (eds), pp. 71–86. Academic Press: New York.
17. Bruce ME, Will RG, Ironside JW, McConnell I, Drummond D, Suttie A *et al* (1997) Transmissions to mice indicate that 'new variant' CJD is caused by the BSE agent. *Nature* **389**:498–501.
18. Chapuis J, Moudjou M, Reine F, Herzog L, Jaumain E, Chapuis C *et al* (2016) Emergence of two prion subtypes in ovine PrP transgenic mice infected with human MM2-cortical Creutzfeldt-Jakob disease prions. *Acta Neuropathol Commun* **4**:10.
19. Clavaguera F, Bolmont T, Crowther RA, Abramowski D, Frank S, Probst A *et al* (2009) Transmission and spreading of tauopathy in transgenic mouse brain. *Nat Cell Biol* **11**:909–913.
20. Collinge J (2016) Mammalian prions and their wider relevance in neurodegenerative diseases. *Nature* **539**:217–226.
21. Collinge J, Clarke AR (2007) A general model of prion strains and their pathogenicity. *Science* **318**:930–936.

22. Collis SC, Kimberlin RH (1985) Long-term persistence of scrapie infection in mouse spleens in the absence of clinical disease. *FEMS Microbiol Lett* **29**:111–114.

23. Comoy EE, Mikol J, Jaffre N, Lebon V, Levavasseur E, Streichenberger N *et al* (2017) Experimental transfusion of variant CJD-infected blood reveals previously uncharacterised prion disorder in mice and macaque. *Nat Commun* **8**:1268.

24. Concha-Marambio L, Pritzkow S, Moda F, Tagliavini F, Ironside JW, Schulz PE, Soto C (2016) Detection of prions in blood from patients with variant Creutzfeldt-Jakob disease. *Sci Transl Med* **8**:370ra183.

25. Diack AB, Head MW, McCutcheon S, Boyle A, Knight R, Ironside JW *et al* (2014) Variant CJD. 18 years of research and surveillance. *Prion* **8**:286–295.

26. Dickinson AG (1976) Scrapie in sheep and goats. In: *In Slow Virus Diseases of Animals and Man*. RH Kimberlin (ed), pp. 209–241. North Holland Publishing: Amsterdam.

27. Dickinson AW, Outram GW, Taylor DM, Foster JD (1986) Further evidence that scrapie agent has an independent genome. In: *Unconventional Virus Diseases of the Central Nervous System*. LA Court, D Dormont, P Brown, DT Kingsbury (eds), pp. 446–460. Commisariat à l'Energie Atomique: Paris, France.

28. Eisele YS, Obermuller U, Heilbronner G, Baumann F, Kaeser SA, Wolburg H *et al* (2010) Peripherally applied Abeta-containing inoculates induce cerebral beta-amyloidosis. *Science* **330**:980–982.

29. Fernandez-Borges ND, Bari MA, Erana H, Sanchez-Martin M, Pirisinu L, Parra B, *et al* (2017) Cofactors influence the biological properties of infectious recombinant prions. *Acta Neuropathol* **135**:179–199.

30. Fournier JG, Kopp N, Streichenberger N, Escaig-Haye F, Langeveld J, Brown P (2000) Electron microsocopy of brain amyloid plaques from a patient with new variant Creutzfeldt-Jakob disease. *Acta Neuropathol* **99**:637–642.

31. Giles K, Olson SH, Prusiner SB (2017) Developing therapeutics for PrP prion diseases. *Cold Spring Harb Perspect Med* **7**:a023747.

32. Gill ON, Spencer Y, Richard-Loendt A, Kelly C, Dabaghian R, Boyes L *et al* (2013) Prevalent abnormal prion protein in human appendixes after bovine spongiform encephalopathy epizootic: large scale survey. *BMJ* **347**:f5675.

33. Glatzel M, Aguzzi A (2000) PrP(C) expression in the peripheral nervous system is a determinant of prion neuroinvasion. *J Gen Virol* **81**:2813–2821.

34. Glatzel M, Giger O, Braun N, Aguzzi A (2004) The peripheral nervous system and the pathogenesis of prion diseases. *Curr Mol Med* **4**:355–359.

35. Glatzel M, Heppner FL, Albers KM, Aguzzi A (2001) Sympathetic innervation of lymphoreticular organs is rate limiting for prion neuroinvasion. *Neuron* **31**:25–34.

36. Gonzalez-Montalban N, Lee YJ, Makarava N, Savtchenko R, Baskakov IV (2013) Changes in prion replication environment cause prion strain mutation. *faseb J* **27**:3702–3710.

37. Hamaguchi T, Eisele YS, Varvel NH, Lamb BT, Walker LC, Jucker M (2012) The presence of Abeta seeds, and not age per se, is critical to the initiation of Abeta deposition in the brain. *Acta Neuropathol* **123**:31–37.

38. Hamaguchi T, Noguchi-Shinohara M, Nozaki I, Nakamura Y, Sato T, Kitamoto T *et al* (2009) The risk of iatrogenic Creutzfeldt-Jakob disease through medical and surgical procedures. *Neuropathology* **29**:625–631.

39. Hamaguchi T, Sakai K, Noguchi-Shinohara M, Nozaki I, Takumi I, Sanjo N *et al* (2013) Insight into the frequent occurrence of dura mater graft-associated Creutzfeldt-Jakob disease in Japan. *J Neurol Neurosurg Psychiatry* **84**:1171–1175.

40. Haybaeck J, Heikenwalder M, Klevenz B, Schwarz P, Margalith I, Bridel C *et al* (2011) Aerosols transmit prions to immunocompetent and immunodeficient mice. *PLoS Pathog* **7**:e1001257.

41. Heggebo R, Press CM, Gunnes G, Ulvund MJ, Tranulis MA, Lsverk T (2003) Detection of PrP(Sc) in lymphoid tissues of lambs experimentally exposed to the scrapie agent. *J Comp Pathol* **128**:172–181.

42. Katorcha E, Makarava N, Savtchenko R, Baskakov IV (2015) Sialylation of the prion protein glycans controls prion replication rate and glycoform ratio. *Sci Rep* **5**:16912.

43. Kimberlin RH, Walker CA (1979) Pathogenesis of mouse scrapie: dynamics of agent replication in spleen, spinal cord and brain after infection by different routes. *J Comp Pathol* **89**:551–562.

44. Kimberlin RH, Walker CA (1986) Pathogenesis of scrapie (strain 263K) in hamsters infected intracerebrally, intraperitoneally or intraocularly. *J Gen Virol* **67**:255–263.

45. Kimberlin RH, Walker CA (1988) Incubation periods in six models of intraperitoneally injected scrapie depend mainly on the dynamics of agent replication within the nervous system and not the lymphoreticular system. *J Gen Virol* **69**:2953–2960.

46. Kimberlin RH, Walker CA (1989) Pathogenesis of scrapie in mice after intragastric infection. *Virus Res* **12**:213–220.

47. Klein MA, Kaeser PS, Schwarz P, Weyd H, Xenarios I, Zinkernagel RM *et al* (2001) Complement facilitates early prion pathogenesis. *Nat Med* **7**:488–492.

48. Klingeborn M, Race B, Meade-White KD, Rosenke R, Striebel JF, Chesebro B (2011) Crucial role for prion protein membrane anchoring in the neuroinvasion and neural spread of prion infection. *J Virol* **85**:1484–1494.

49. Langer F, Eisele YS, Fritschi SK, Staufenbiel M, Walker LC, Jucker M (2011) Soluble Abeta seeds are potent inducers of cerebral beta-amyloid deposition. *J Neurosci* **31**:14488–14495.

50. Liberski PP, Sikorska B, Hauw JJ, Kopp N, Streichenberger N, Giraud P *et al* (2010) Ultrastructural characteristics (or evaluation) of Creutzfeldt-Jakob disease and other human transmissible spongiform encephalopathies or prion diseases. *Ultrastruct Pathol* **34**:351–361.

51. Llewelyn CA, Hewitt PE, Knight RS, Amar K, Cousens S, Mackenzie J, Will RG (2004) Possible transmission of variant Creutzfeldt-Jakob disease by blood transfusion. *Lancet* **363**:417–421.

52. Luk KC, Kehm VM, Zhang B, O'Brien P, Trojanowski JQ, Lee VMY (2012) Intracerebral inoculation of pathological alpha-synuclein initiates a rapidly progressive neurodegenerative alpha-synucleinopathy in mice. *J Exp Med* **209**:975–986.

53. Magnusson K, Simon R, Sjolander D, Sigurdson CJ, Hammarstrom P, Nilsson KP (2014) Multimodal fluorescence microscopy of prion strain specific PrP deposits stained by thiophene-based amyloid ligands. *Prion* **8**:319–329.

54. Makarava N, Baskakov IV (2013) The evolution of transmissible prions: the role of deformed templating. *PLoS Pathog* **9**:e1003759.

55. Mochizuki Y, Mizutani T, Tajiri N, Oinuma T, Nemoto N, Kakimi S, Kitamoto T (2003) Creutzfeldt-Jakob disease with florid plaques after cadaveric dura mater graft. *Neuropathology* **23**:136–140.

56. Moda F, Gambetti P, Notari S, Concha-Marambio L, Catania M, Park KW *et al* (2014) Prions in the urine of patients with variant Creutzfeldt-Jakob disease. *N Engl J Med* **371**:530–539.

57. Moore RC, Hope J, McBride PA, McConnell I, Selfridge J, Melton DW, Manson JC (1998) Mice with gene targeted prion protein alterations show that Prnp, Sinc and Prni are congruent. *Nat Genet* **18**:118–125.

58. Nyström S, Bäck M, Nilsson KP, Hammarström P (2017) Imaging amyloid tissues stained with luminescent conjugated oligothiophenes by hyperspectral confocal microscopy and fluorescence lifetime imaging. *J Vis Exp* **128**:e56279.

59. Peden A, McCardle L, Head MW, Love S, Ward HJ, Cousens SN *et al* (2010) Variant CJD infection in the spleen of a neurologically asymptomatic UK adult patient with haemophilia. *Haemophilia* **16**:296–304.

60. Peden AH, Head MW, Ritchie DL, Bell JE, Ironside JW (2004) Preclinical vCJD after blood transfusion in a PRNP codon 129 heterozygous patient. *Lancet* **364**:527–529.

61. Peden AH, Ironside JW (2004) Review: pathology of variant Creutzfeldt-Jakob disease. *Folia Neuropathol* **42** (Suppl A): 85–91.

62. Polymenidou M, Moos R, Scott M, Sigurdson C, Shi YZ, Yajima B *et al* (2008) The POM monoclonals: a comprehensive set of antibodies to non-overlapping prion protein epitopes. *PLoS One* **3**:e3872.

63. Polymenidou M, Stoeck K, Glatzel M, Vey M, Bellon A, Aguzzi A (2005) Coexistence of multiple PrPSc types in individuals with Creutzfeldt-Jakob disease. *Lancet Neurol* **4**:805–814.

64. Prinz M, Heikenwalder M, Junt T, Schwarz P, Glatzel M, Heppner FL *et al* (2003) Positioning of follicular dendritic cells within the spleen controls prion neuroinvasion. *Nature* **425**:957–962.

65. Prinz M, Huber G, Macpherson AJ, Heppner FL, Glatzel M, Eugster HP *et al* (2003) Oral prion infection requires normal numbers of Peyer's patches but not of enteric lymphocytes. *Am J Pathol* **162**: 1103–1111.

66. Prusiner SB (1982) Novel proteinaceous infectious particles cause scrapie. *Science* **216**:136–144.

67. Sigurdson CJ, Manco G, Schwarz P, Liberski P, Hoover EA, Hornemann S *et al* (2006) Strain fidelity of chronic wasting disease upon murine adaptation. *J Virol* **80**:12303–12311.

68. O'Rourke KI, Miller MW, Hoover EA, Spraker TR, Sigurdson CJ, Williams ES (1999) Oral transmission and early lymphoid tropism of chronic wasting disease PrPres in mule deer fawns (Odocoileus hemionus). *J Gen Virol* **80**:2757–2764.

69. Srivastava S, Makarava N, Katorcha E, Savtchenko R, Brossmer R, Baskakov IV (2015) Post-conversion sialylation of prions in lymphoid tissues. *Proc Natl Acad Sci U S A* **112**:E6654–E6662.

70. Taraboulos A, Jendroska K, Serban D, Yang SL, DeArmond SJ, Prusiner SB (1992) Regional mapping of prion proteins in brain. *Proc Natl Acad Sci U S A* **89**:7620–7624.

71. Wadsworth JDF, Joiner S, Hill AF, Campbell TA, Desbruslais M, Luthert PJ, Collinge J (2001) Tissue distribution of protease resistant prion protein in variant CJD using a highly sensitive immuno-blotting assay. *Lancet* **358**:171–180.

72. Wroe SJ, Pal S, Siddique D, Hyare H, Macfarlane R, Joiner S *et al* (2006) Clinical presentation and pre-mortem diagnosis of variant Creutzfeldt-Jakob disease associated with blood transfusion: a case report. *Lancet* **368**:2061–2067.

SUPPORTING INFORMATION

Additional supporting information may be found online in the Supporting Information section at the end of the article.

Figure S1. *Subfibrillar and fibrillar prions replicate early in the spleen after IV inoculation.* Splenic cryosections immunolabeled for PrP (histoblots) reveal similar diffuse aggregates within the follicular germinal centers for all the strains. No PrP immunolabeling was detected in the spleen of mock mice. The spleens were collected from mice at early timepoints post-inoculation (pre-clinical) (RML: 60 dpi; ME7: 48 dpi; mCWD: 89 dpi; 22L 110 dpi; 87V 150 dpi; mock 89 dpi).

Figure S2. *Thermal denaturation of 87V and mCWD prions from mice inoculated IC or from the IV-to-IC subpassage.* A,B. PK-digested brain samples in an SDS-based loading dye were subjected to temperatures from 25°C to 99°C and immediately loaded onto a polyacrylamide gel and electrophoresed. PrP^{Sc} monomers were detected by immunoblotting and the monomer levels were quantified at each temperature. The PrP signal measured at 99°C was considered as total PrP^{Sc} (100%). Graphs show the mean $\pm$ standard error (SE) of PrP^{Sc} from IC-inoculated 87V and mCWD (black) and the IV-to-IC subpassage (red) at each temperature. $T_{1/2}$ was calculated from a nonlinear logistic regression curve. **A.** The $T_{1/2}$ for the 87V IC and the 87V IV-to-IC PrP^{Sc} were 89.0°C $\pm$ 0.9°C and 85.6°C $\pm$ 1.6°C, respectively, with no significant differences between the groups. **B.** The $T_{1/2}$ for the mCWD IC was 81.6°C $\pm$ 1.1°C. The PrP^{Sc} levels from the mCWD IV-to-IC infected mice are generally low and the thermostability was conclusive only in the mouse shown with a calculated $T_{1/2}$ of 80.9°C. n = 4 mice for 87V IC and IV-to-IC and n = 3 for mCWD IC.